Research Article | Vol. 25, No. 13 | 26 Jun 2017 | OPTICS EXPRESS 14059
Optics EXPRESS

Helicity-dependent forked vortex lens based on photo-patterned liquid crystals

WEI DUAN, PENG CHEN, SHI-JUN GE, BING-YAN WEI, WEI HU,* AND YAN-QING LU

National Laboratory of Solid State Microstructures, College of Engineering and Applied Sciences, and Collaborative Innovation Center of Advanced Microstructures, Nanjing University, Nanjing 210093, China
*huwei@nju.edu.cn

Abstract: A liquid crystal forked vortex lens integrated with Pancharatnam-Berry phase is proposed and demonstrated via a dynamic photo-patterning technique. The forked vortex lens can generate two optical vortices with opposite spin and orbital angular momentum, which are spatially separated to two focal points with one optical vortex focused and the other defocused. It exhibits distinctive helicity-dependency and ultra-high diffraction efficiency up to 95%. The topological charges of generated optical vortices are detected via astigmatic transformation. This work supplies an easy fabrication and low power consumption strategy for generating and separating (de-)focused optical vortices simultaneously.

OCIS codes: (160.3710) Liquid crystals; (230.3720) Liquid-crystal devices; (050.1965) Diffractive lenses; (050.4865) Optical vortices; (260.5430) Polarization.

References and links

1. S. Sato, "Liquid-crystal lens-cells with variable focal length," Jpn. J. Appl. Phys. **18**(9), 1679–1684 (1979).
2. H. Ren and S. T. Wu, *Introduction to Adaptive Lenses* (John Wiley, 2012).
3. Y. Li and S. T. Wu, "Polarization independent adaptive microlens with a blue-phase liquid crystal," Opt. Express **19**(9), 8045–8050 (2011).
4. Y. H. Lin and H. S. Chen, "Electrically tunable-focusing and polarizer-free liquid crystal lenses for ophthalmic applications," Opt. Express **21**(8), 9428–9436 (2013).
5. H. S. Chen, Y. J. Wang, P. J. Chen, and Y. H. Lin, "Electrically adjustable location of a projected image in augmented reality via a liquid-crystal lens," Opt. Express **23**(22), 28154–28162 (2015).
6. X. Q. Wang, F. Fan, T. Du, A. M. W. Tam, Y. Ma, A. K. Srivastava, V. G. Chigrinov, and H. S. Kwok, "Liquid crystal Fresnel zone lens based on single-side-patterned photoalignment layer," Appl. Opt. **53**(10), 2026–2029 (2014).
7. N. V. Tabiryan, S. V. Serak, S. R. Nersisyan, D. E. Roberts, B. Y. Zeldovich, D. M. Steeves, and B. R. Kimball, "Broadband waveplate lenses," Opt. Express **24**(7), 7091–7102 (2016).
8. L. Allen, M. W. Beijersbergen, R. J. Spreeuw, and J. P. Woerdman, "Orbital angular momentum of light and the transformation of Laguerre-Gaussian laser modes," Phys. Rev. A **45**(11), 8185–8189 (1992).
9. A. M. Yao and M. J. Padgett, "Orbital angular momentum: origins, behavior and applications," Adv. Opt. Photonics **3**(2), 161–204 (2011).
10. X. L. Wang, X. D. Cai, Z. E. Su, M. C. Chen, D. Wu, L. Li, N. L. Liu, C. Y. Lu, and J. W. Pan, "Quantum teleportation of multiple degrees of freedom of a single photon," Nature **518**(7540), 516–519 (2015).
11. J. Wang, "Advances in communications using optical vortices," Photonics Res. **4**(5), B14–B28 (2016).
12. M. Padgett and R. Bowman, "Tweezers with a twist," Nat. Photonics **5**(6), 343–348 (2011).
13. A. M. Tam, F. Fan, T. Du, W. Hu, W. L. Zhang, C. X. Zhao, X. Q. Wang, K. L. Ching, G. J. Li, H. L. Luo, V. Chigrinov, S. C. Wen, and H. S. Kwok, "Bifocal optical-vortex lens with sorting of the generated nonseparable spin-orbital angular-momentum states," Phys. Rev. Appl. **7**(3), 0304010 (2017).
14. W. Duan, P. Chen, B. Y. Wei, S. J. Ge, X. Liang, W. Hu, and Y. Q. Lu, "Fast-response and high-efficiency optical switch based on dual-frequency liquid crystal polarization grating," Opt. Mater. Express **6**(2), 597–602 (2016).
15. A. M. Tam, F. Fan, H. S. Chen, T. Du, V. G. Chigrinov, Y. H. Lin, and H. S. Kwok, "Nanoscopic patterned photo-alignment for electrically switchable liquid crystal Pancharatnam-Berry phase diffractive lens," J. Soc. Inf. Disp. **47**, 599–601 (2016).
16. S. Pancharatnam, "Generalized theory of interference, and its applications. Part I. Coherent pencils," Proc. Indian Acad. Sci. A **44**, 247–262 (1952).
17. M. V. Berry, "The adiabatic phase and Pancharatnam's phase for polarized light," J. Mod. Opt. **34**(11), 1401–1407 (1987).

#293231 https://doi.org/10.1364/OE.25.014060
Journal © 2017 Received 21 Apr 2017; revised 2 Jun 2017; accepted 3 Jun 2017; published 12 Jun 2017

Optics EXPRESS

18. P. Chen, B. Y. Wei, W. Ji, S. J. Ge, W. Hu, F. Xu, V. Chigrinov, and Y. Q. Lu, "Arbitrary and reconfigurable optical vortex generation: a high-efficiency technique using director-varying liquid crystal fork gratings," Photonics Res. **3**(4), 133–139 (2015).
19. Y. Ke, Z. Liu, Y. Liu, J. Zhou, W. Shu, H. Luo, and S. Wen, "Compact photonic spin filters," Appl. Phys. Lett. **109**(18), 181104 (2016).
20. H. Wu, W. Hu, H. C. Hu, X. W. Lin, G. Zhu, J. W. Choi, V. Chigrinov, and Y. Q. Lu, "Arbitrary photo-patterning in liquid crystal alignments using DMD based lithography system," Opt. Express **20**(15), 16684–16689 (2012).
21. B. Y. Wei, W. Hu, Y. Ming, F. Xu, S. Rubin, J. G. Wang, V. Chigrinov, and Y. Q. Lu, "Generating switchable and reconfigurable optical vortices via photopatterning of liquid crystals," Adv. Mater. **26**(10), 1590–1595 (2014).
22. V. Chigrinov, S. Pikin, A. Verevochnikov, V. Kozenkov, M. Khazimullin, J. Ho, D. D. Huang, and H. S. Kwok, "Diffusion model of photoaligning in azo-dye layers," Phys. Rev. E Stat. Nonlin. Soft Matter Phys. **69**(6), 061713 (2004).
23. V. Denisenko, V. Shvedov, A. S. Desyatnikov, D. N. Neshev, W. Krolikowski, A. Volyar, M. Soskin, and Y. S. Kivshar, "Determination of topological charges of polychromatic optical vortices," Opt. Express **17**(26), 23374–23379 (2009).
24. M. J. Tang, P. Chen, W. L. Zhang, A. M. Tam, V. G. Chigrinov, W. Hu, and Y. Q. Lu, "Integrated and reconfigurable optical paths based on stacking optical functional films," Opt. Express **24**(22), 25510–25514 (2016).
25. L. Tan, J. Y. Ho, and H. S. Kwok, "Extended Jones matrix method for oblique incidence study of polarization gratings," Appl. Phys. Lett. **101**(5), 051107 (2012).

1. Introduction

Liquid crystals (LCs) are promising candidates for the tunable and dynamic optical elements due to their large birefringence and continuous external field tunability. Among them, LC lens has sparked significant interests in the thriving fields of ophthalmic apparatuses and augmented reality displays, *etc* [1–5]. However, the traditional electrically tunable LC lenses require delicate electrodes and constant power consumption to reorient and keep LC directors [2]. Fresnel lenses based on binary azimuthal angle control have been demonstrated by photo-alignment techniques, with diffraction efficiency theoretically limited to 41% [6]. More recently, Pancharatnam-Berry (PB) phase is introduced to realize a continuous lens phase profile, thus pushing the limit to 100% [7].

Optical vortex, featured by a phase singularity and helical phase front, has been extensively studied during the past two decades. Its screw-type phase distribution leads to an orbital angular momentum (OAM) of $m\hbar$ per photon [8], wherein m represents the topological charge. Such specific beam plays an important role in particle manipulation, optical communication, quantum information and computation [9, 10]. Especially in OAM based mode division multiplexing and optical tweezers [11, 12], lenses are indispensable for beam coupling and focusing. Recently, a vortex lens that combines the functions of vortex beam generator and lens is proposed to generate (de-)focused vortex beam [13]. The two generated vortices are coaxial and nonseparable, a separating process is thus indispensable.

Here, by introducing a blazed PB phase [14], we propose polarization forked vortex lens (PFVL) which can separate (de-)focused vortices spatially. The PFVL is essentially an inhomogeneous wave plate whose optical axis distribution is an integration of a PB lens and a polarization forked grating. Corresponding diffraction properties are theoretically analyzed. A dynamic LC photo-patterning technique is employed for the PFVL fabrication. The PFVL can generate two focused/defocused optical vortices with opposite spin and OAM, which are spatially separated to two focal points. Meanwhile, the focusing characteristics are dependent on the propagation direction of incident light [15]. A high diffraction efficiency up to 95% is obtained. This work provides a strategy with compact configuration and multifunction of optical vortices generating, separating, and focusing.

2. Principle and fabrication

The PFVL can locally modulate the incident polarization states and result in space-variant output phases, namely PB phase [16, 17]. Its optical axis distribution is an integration of a

polarization forked grating [18] and a PB lens [19].The optical axes are homogeneous along *z* axis and obey the following equation in the *x*-*y* plane:

$$\alpha = -\pi x/\Lambda + \frac{1}{2}m\varphi + \frac{\pi}{\lambda}\left(\sqrt{r^2 + f^2} - f\right), \tag{1}$$

where $\varphi = \arctan(y/x)$ is the azimuthal angle, m is the topological charge, Λ is the pitch, $r^2 = x^2 + y^2$, r is the radius, and f is the focal length. Figures 1(a)-1(c) show the calculated director distributions of the PFVL with f = 10 cm and m = 1, 2, 8, respectively. The gradient color variation from blue to red indicates the optical axis orientation varying from 0 to π continuously.

The transformation in a PFVL can be analyzed through Jones matrix calculation. The transfer matrix is:

$$\begin{aligned}\mathbf{T} &= \mathbf{R}(-\alpha)\cdot\begin{bmatrix}\exp(-i\Gamma/2) & 0\\ 0 & \exp(i\Gamma/2)\end{bmatrix}\cdot\mathbf{R}(\alpha)\\ &= \cos\frac{\Gamma}{2}\mathbf{I} - i\sin\frac{\Gamma}{2}\begin{bmatrix}\cos 2\alpha & \sin 2\alpha\\ \sin 2\alpha & -\cos 2\alpha\end{bmatrix},\end{aligned} \tag{2}$$

where $\Gamma = 2\pi\Delta nd/\lambda$ is the phase retardation, Δn is the LC birefringence, d is the cell gap, and λ indicates the free space wavelength. Considering a circular incident polarization, it can be described as $\mathbf{E}_{\text{in}} = \chi^{(\pm)} = 1/\sqrt{2}\begin{pmatrix}1 & \pm i\end{pmatrix}^{\mathrm{T}}$, the two spin eigenstates corresponding to left (+) and right (–) circular polarization states, respectively. After passing through the PFVL, the output can be expressed as:

$$\mathbf{E}_{out} = \mathbf{T}\cdot\mathbf{E}_{\text{in}} = \cos\frac{\Gamma}{2}\cdot\chi^{(\pm)} - i\sin\frac{\Gamma}{2}\cdot\exp\left[\pm im\varphi \mp i2\pi x/\Lambda \pm i\frac{2\pi}{\lambda}\left(\sqrt{r^2 + f^2} - f\right)\right]\cdot\chi^{(\mp)}. \tag{3}$$

For a right circularly polarized (RCP) incident beam, the output is a superposition of two parts: the residual RCP component (0th order), and the transformed left circularly polarized (LCP) one (−1st order, defined as the first order on the left side along the propagation of the incident light) with a spiral phase factor exp(-*im*φ), a tilted phase factor exp(*i*2π*x*/Λ), and a spherical phase factor exp{-*i*2π[$(r^2 + f^2)^{1/2}$-*f*]/λ}, corresponding to an off-axial focused helical optical vortex. On the other hand, for LCP condition, the transformed RCP (+ 1st order, defined as the first order on the right side) is a defocused optical vortex with opposite OAM and diffracted direction. Under half-wave condition (Γ = π, 3π, 5π…), the residual component is totally suppressed and the output wave is a pure helical beam. Therefore, for circular polarization, the input will be theoretically 100% diffracted to a single first order. While for linearly polarized incident light, it will be equally diffracted to ± 1st orders with focused and defocused states, respectively.

A digital micro-mirror device based dynamic microlithography system [20, 21] is utilized to implement the photo-patterning on a polarization sensitive photoalignment agent, which is 0.3% solution of sulphonic azo-dye SD1 (Dai-Nippon Ink and Chemicals, Japan) in dimethylformamide spin coated on indium-tin-oxide glass substrates. To satisfy the half-wave condition for incident wavelength λ = 633 nm, 5 μm spacers are selected to keep the cell gap. Then, the cell is placed at the image plane of the system to record the designed patterns. The SD1 molecules tend to reorient their absorption oscillators perpendicular to the UV light polarization [22]. After an eighteen-step five-time-partly-overlapping UV exposure [18], the LC material (E7, HCCH, China) is capillarily filled, thus, the PFVL is accomplished.

Optics EXPRESS

3. Results and discussions

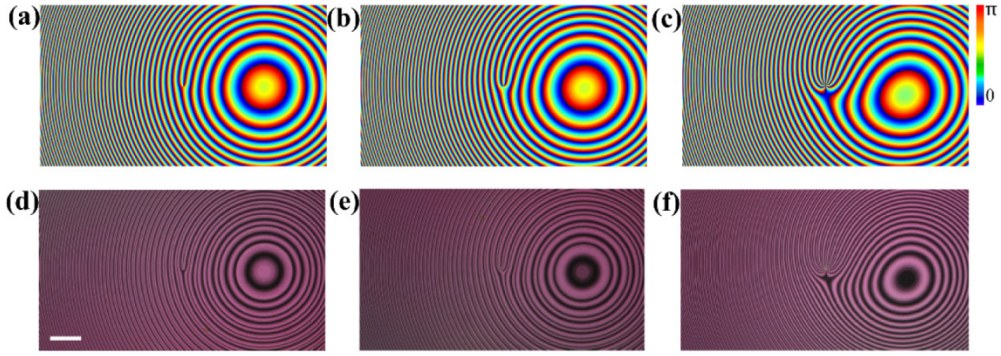

Fig. 1. The theoretical director distributions (a)-(c) and corresponding micrographs (d)-(f) of PFVLs with m = 1, m = 2 and m = 8, respectively. The scale bar is 200 μm.

The micrographs of the obtained LC PFVLs under a polarized optical microscope are shown in Figs. 1(d)-1(f). The continuous variation of the brightness gives a vivid exhibition of the space-variant directors. The dark domains correspond to regions with LC directors approximately perpendicular to the polarizer or analyzer, whereas the bright domains correspond to regions with LC directors around 45° with respect to the polarizer or analyzer. The bright-to-dark alternates twice when the director changes from 0 to π, leading to denser fringes under the microscope. The similar patterns and gradually changed brightness reveal that the designed PFVLs are faithfully transferred into the LC cells.

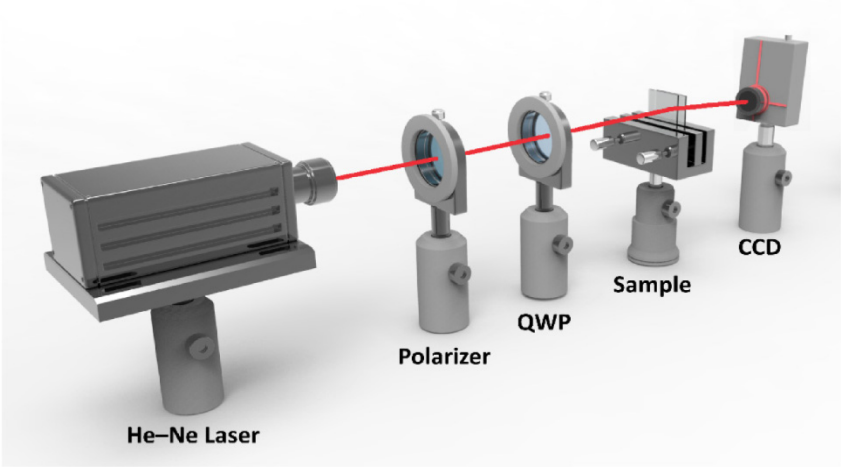

Fig. 2. Scheme of the optical setup for generating and detecting (de-)focused vortices.

To characterize the performance of the PFVL, several tests have been carried out. As shown in Fig. 2, a 633 nm He-Ne laser beam passes through a polarizer, a quarter wave-plate (QWP) and then illuminates on the sample with the transmitted light captured by a CCD. The angle between the c-axis of the QWP and the polarization direction is set to be + 45°/- 45° to get RCP/LCP. The focused/defocused optical vortex is thus generated. The measured focal length is f = 10.08 cm, which is consistent with the designed f.

Optics EXPRESS

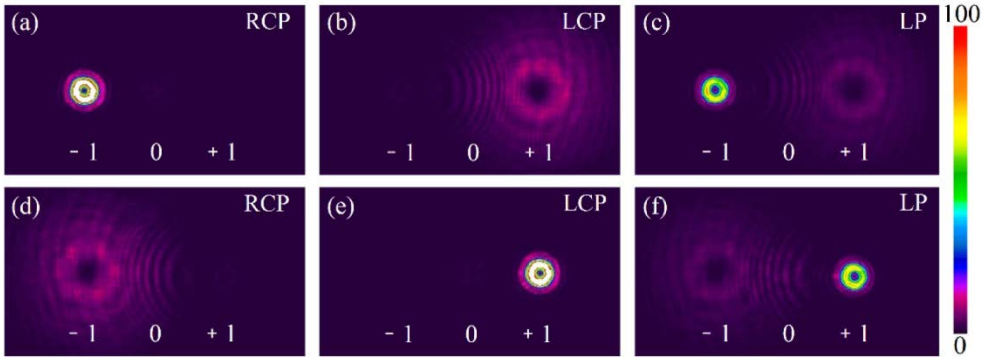

Fig. 3. The intensity images of generated focused/defocused vortex beams corresponding to (a) RCP, (b) LCP and (c) linearly polarized incident beams. (d)-(f) show the images corresponding to the horizontally flipped samples.

The diffraction properties of a PFVL with $m = 2$ is measured. As expected, for the RCP incident beam, a focused vortex beam is observed on the −1st order. As shown in Fig. 3(a), only a single order exists, indicating the half-wave condition is perfectly satisfied ($\Gamma = 3\pi$). The intensity profile is donut-like owing to the phase singularity at the center of the beam. Figure 3(b) reveals a defocused vortex beam is generated on the + 1st order for LCP incident beam. For linear polarization, the beam energy is equally diffracted to ± 1st orders, as presented in Fig. 3(c). Obviously, switching among above three states could be realized via adjusting the incident polarization. The results are consistent with the previous theoretical analyses. Subsequently, we horizontally flip the sample and find that the sample exhibits reversed focusing characteristics with other features unchanged, which is revealed in Figs. 3(d)-3(f). For instance, the incident RCP beam is transformed to a defocused LCP vortex beam, whose intensity distribution is shown in Fig. 3(d). To verify the topological charges of the generated focused vortices, a cylindrical lens is employed to implement the astigmatic transformation [23, 24]. Figures 4(a)-4(c) present the converted patterns where the numbers of dark stripes (marked by white dash lines) indicate corresponding topological charges (m = 1, 2, 8) of the PFVLs shown in Figs. 1(a)-1(c). The defocused orders are also characterized, and the converted patterns exhibit the same numbers of dark stripes with symmetric tilt directions (m = –1, –2, –8).

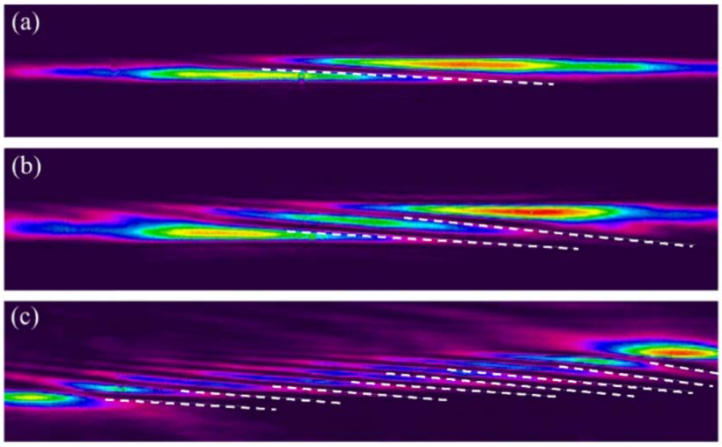

Fig. 4. The astigmatic transformation of optical vortices with (a) m = 1, (b) m = 2 and (c) m = 8.

Optics EXPRESS

Herein, the proposed PFVLs can generate helicity-dependent focused/defocused optical vortices. Additionally, the vortices with opposite spin and OAM are separated spatially. To obtain the maximum efficiency, normal incidence is required. The oblique incidence will lead to lower power efficiency [25]. The diffraction efficiency is defined as the ratio between the single objective order (both first orders) and the total transmittance for circular (linear) incident polarization. All the measured efficiencies are ~95% and the efficiencies for LCP and RCP beams are equal in case of linear incident polarization. The multifunctional PFVLs also exhibit the merits of low power consumption, easy fabrication and broadband tunability. It may supply a compact and practical strategy for the vortex beam coupling and focusing in OAM based mode division multiplexing and optical tweezers.

4. Conclusion

In this work, an LC polarization forked vortex lens is proposed and demonstrated via a dynamic photo-patterning technique. It is an inhomogeneous wave plate with specific optical axis distribution, which is an integration of a PB lens and a polarization forked grating. The PFVL can generate and separate (de-)focused optical vortices simultaneously. Thanks to its advantages of helicity dependency and high efficiency, the proposed PFVL supplies a practical approach for (de-)focused vortex generation and prompts various applications in optical manipulation and communication.

Funding

This work was sponsored by the National Natural Science Foundation of China (NSFC) programs (Nos. 61490714, 61435008 and 61575093).